University of Baghdad
College of Engineering
JE
JOURNAL OF ENGINEERING

Journal of Engineering
journal homepage: www.joe.uobaghdad.edu.iq
Number 11 Volume 25 November 2019

Mechanical and Energy Engineering

Prediction of Heat Transfer Coefficient and Pressure Drop in Wire Heat Exchanger Working with R-134a and R-600a

Dr. Louay Abd Al-Azez Mahdi*
Asst.Prof.
Mechanical Engineering
University of Technology
E-mail: louayalkaesy@gmail.com
20035@technology.edu.iq

Ahmed Yusef Lateif
MSc. Student
Mechanical Engineering
University of Technology
E-mail: ahmed.yusef.1993@gmail.com

ABSTRACT

An experimental and theoretical works were carried out to model the wire condenser in the domestic refrigerator by calculating the heat transfer coefficient and pressure drop and finding the optimum performance. The two methods were used for calculation, zone method, and an integral method. The work was conducted by using two wire condensers with equal length but different in tube diameters, two refrigerants, R-134a and R-600a, and two different compressors matching the refrigerant type. In the experimental work, the optimum charge was found for the refrigerator according to ASHRAE recommendation. Then, the tests were done at 32˚C ambient temperature in a closed room with dimension (2m*2m*3m). The results showed that the average heat transfer coefficient for the R-600a was higher than the R-134a, so the length of the wire tube was longer with R-134a than R-600a. The pressure drop for the smaller tube diameter was higher than the other tube .The second law thermodynamic efficiency was higher for R-600a, which reached 41% . The entropy generation minimization analysis showed that the R-600a refrigerant type and smaller tube diameter are approached the optimum point.

Keywords: wire condenser, heat transfer coefficient, pressure drop.

التنبؤ بمعامل انتقال الحرارة وهبوط الضغط لمبادل حراري سلكي يعمل مع وسيط تبريد R-600a و R-134a

أ.م.د لؤي عبد العزيز مهدي
قسم الهندسة الميكانيكية
الجامعة التكنولوجية

طالب الماجستير احمد يوسف لطيف
قسم الهندسة الميكانيكية
الجامعة التكنولوجية

الخلاصة

في العمل الحالي ، تم تنفيذ الأعمال التجريبية والنظرية لنمذجة المكثف السلكي في الثلاجة المنزلية عن طريق حساب معامل انتقال الحرارة وانخفاض الضغط وإيجاد أفضل أداء للنظام باستخدام طريقتين: طريقة المقاطع وطريقة التكامل. تم إنجاز العمل باستخدام مكثفين سلكين بطول متساوٍ ولكن قطر الأنبوب مختلف ، و استعمال مائعي التبريد R-134a و R-600a ، واثنين من الضواغط المختلفة التي تتطابق مع نوع مائع التبريد. في بداية العمل التجريبي تم ايجاد الشحنة المثلى للثلاجة وفقا لتوصية ASHRAE والاختبارات أجريت عند درجة حرارة 32 درجة مئوية في غرفة مغلقة مع أبعاد (2 م * 2 م * 3 م).اظهرت النتائج ان متوسط معامل انتقال الحرارة لـ R-600a أعلى من R-134a ، لذا فإن طول الأنبوب السلكي لـ R-134a اكبر من R-600a. كان انخفاض الضغط للأنبوب الاقل قطرا أعلى من الأنبوب الآخر. إن الكفاءة الديناميكية الحرارية للقانون الثاني عالية بالنسبة لـ R-600a التي

*Corresponding author
Peer review under the responsibility of University of Baghdad.
https://doi.org/10.31026/j.eng.2019.11.01

Article received: 18/11/2018
Article accepted: 16/1/2019
Article published: 1/11/2019

وصلت إلى 41٪. يبين تحليل التقليل من توليد الإنتروبـي أن نـوع المكثـف السـلكي ل R-600a مـع قطـر الأنبـوب الاقـل قطـرا هـو الأقرب إلى النقطة المثلى.

الكلمات الرئيسية: المكثف السلكي, معامل انتقال الحرارة, هبوط الضغط.

1. INTRODUCTION

The static condenser is used due to it's low cost and simple construction. Also, it's performance is affected by the environment and the other components of the system. The study of wire condenser is very important, and clarifying it's thermal behavior is the key to improve, especially for the saturated region. Theoretical and experimental work will be used to calculate the heat transfer coefficient and pressure drop in the condenser in three regimes (superheated, saturated, subcooled). Also, it shows the different performances of the used different refrigerants and different tube diameters of condenser, to optimize the condenser required to remove heat from refrigerant to air. This will be done by finding the flow pattern type and selecting the governing equations to calculate the heat transfer coefficient and the pressure drop in a detailed manner as well as to calculate the length of the heat exchangers, but few were directed to the static condenser as follows:-

Ragazzi, and Pedersen, 1991 developed a computer simulation modeling to optimize the air-cooled condenser with the refrigerants R-12 and R-134a. The study used two methods to calculate the heat transfer coefficient and pressure drop in the condenser. The first method was fixed length, and the second method was fixed quality. This method works well for two-phase only. The result depicted that the refrigerant R-12 had more efficiency than refrigerant R-134a, but the refrigerant R-134a showed less damage to the ozone layer. **El Hajal, et al., 2003** performed an experimental analysis work for condensation in horizontal tubes depending on the model of a two-phase flow pattern map. The experimental work was done with different refrigerants and for the following range of limitations: mass velocities from 24 to 1022 kg/m^2sec, tube internal diameters from 3.1 to 21.4 mm and vapor qualities from 0.03 to 0.97. The results displayed the maps of flow patterns region of all these refrigerants and determination of transition regions of flow patterns. **Tanda, and Tagliafico, 1997** presented an experimental work to predict the natural convection and radiation heat despite from the external surface of the vertical wire-and-tube condenser and using water as a refrigerant. The study found the effects of the most important geometric and operating parameters, like the overall height of the exchanger, the spacing-to-diameter ratios of tubes and wires, and the mean tube to air temperature difference. Also, it was found that the radiation heat transfer represented 15% of the total heat transfer. **Bansal, and Chin**, **2003** carried out modeling and experimental study for the wire-and-tube condenser. A simulation model was developed using the finite element and variable conductance approach with a combination of thermodynamic correlations. The results showed that the outer heat transfer resistance contributed to about 80 and 83-95% of the total heat transfer for a single and two-phase flow, respectively and the heat transfer mode for wire-condenser was by convection, which contributed up to 65% of the total heat transfer. **Dagilis, and Hofmanas, 2012** carried out experimental and numerical investigations to determine the influence of surrounding space around the condenser of a household refrigerator on the heat transfer efficiency. The study decision was a better performance done when more space for the condenser. In the experimental work, the condensing temperature was fixed at 40.3˚C, but when the condenser was bent to avoid the heat influence from the compressor shell, the condensing temperature reduced to 36.7˚C. The results indicated that the external heat transfer coefficient could rise by 14% in the case when the condenser was fully free and by 9% if the space between the condenser and wall-room was enlarged by 0.3 m. **Heo, et al., 2012** presented an experimental work done to study the influence of vertical and horizontal pitches on the natural convection of two vertically staggered cylinders for both laminar and turbulent flows. The experimental work was conducted by varying the vertical and horizontal pitch-to-diameter ratios using a copper electroplating system, and the numerical simulations were performed using the FLUENT program. The results displayed that the heat transfer of the lower cylinder was similar to the single cylinder and demonstrated the effects of preheating, velocity, and side-flow from the lower cylinder on the upper cylinder. These effects weakened with increasing horizontal pitch-to-diameter ratio. **Melo, and Hermes, 2009** conducted an analysis and experimental work to estimate the heat transfer coefficient between the external surfaces of natural draft wire-and-tube condensers and the surrounding air. The Buckingham-Pi theorem was used to derive a dimensionless multiplier in terms of the working temperatures and heat exchanger geometry, and this correlation predicted 79% of the measured data within an error band of +5%. **Lee, and Son, 2010** experimentally tested a horizontal double pipe heat exchanger. The work used the refrigerants R-290, R-600a, R-22 and R-134a and different inner diameters 10.07, 7.73, 6.54, and 5.8 mm, and mass flux varying from 35.5 to 210.4 kg/m^{2}sec. The results illustrated that the average condensation heat transfer coefficients of R-600a and R-290 were higher than those of R-134a and R-22, and the pressure drops of the four refrigerants were R-600a>R-290>R-134a > R-22. Also, the heat transfer coefficient of refrigerant was higher at 5.8 mm tube diameter and lower at 10.07 mm tube diameter for all the above refrigerants.

Most of the researches don't cover all the details of pressure drop or the equations that were used to determine the pressure drop. The current work will be done to find a thermodynamic analysis for the wire condenser for refrigerant side and airside depending on the entropy generation minimization theory for A. Bejan.

2. EXPERIMENTAL WORK

2.1 Domestic Refrigerator

The domestic refrigerator used in the experimental work is shown in **Fig. 1**. It consists of a cabinet, a reciprocating compressor, a wire condenser, a roll bond evaporator, and a capillary tube. The refrigerator is made of pressed steel with paint and waterproof outside shell. The specifications of the main components are as follows; the two hermetic reciprocating compressors working with different refrigerant; the first compressor is working with R-134a refrigerant, with flow capacity is 8.1cm^3, and cooling capacity is 210W, and the second is working with R-600a, with flow capacity of 11.2cm^3, and cooling capacity of 198W. Both the compressors are working according to **ASHRAE, 1997.** The lengths of condensers were used in the experimental test is 10.25m with different tube diameters (4.76 mm and 6.35 mm). The evaporator is a roll-bond. The optimum inner diameter and length of the capillary tube are (0.66 mm) and (1.17 m), respectively. The cabinet size is 10 cubic feet. The back of the cabinet was covered with aluminum foil to prevent the heat transfer to the cabinet by radiation from the wire condenser. Also, the space between the frame and the door of cabinet was covered with a magnetic gasket to prevent heat loss and air infiltration.

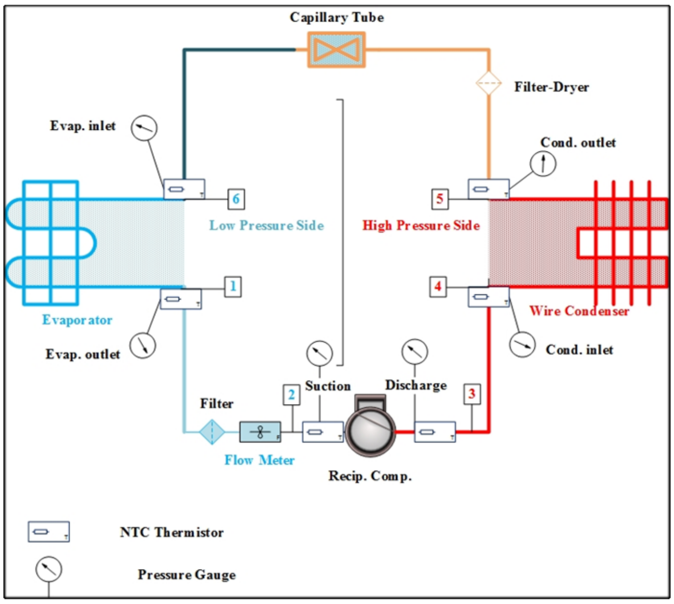

Figure 1. The diagram of the system and instrumentation.

2.2 Instrumentation

Several measuring instruments have been used with domestic refrigerator. Thermistors of negative temperature coefficient (NTC) type are used to measure the temperature. The pressure gauges were used to indicate the pressure at high and low-pressure sides of the refrigerant circuit. Also, four pressure transducers were used to measure the pressure across the compression cycle of the domestic refrigerator. A turbine refrigerant volume flow meter made from stainless steel was used to measure the flow rate of refrigerant. Digital power clamp meter was used to measure the current; the voltage supplied to the refrigerator, and the power consumption per hour and day. The electronic refrigerant scale was used to measure the refrigerant mass inventory of the domestic refrigerator. All the measuring devices are connected with interface unit Data Acquisition DAQ (Arduino MEGA 2560). The interface Arduino connected to the computer control system (Laptop) to view the data using LABVIEW software, which enables the communication between the systems under study. The refrigerants were charged using an electronic scale to measure the required amount of refrigerant mass.

3. STATIC CONDENSER MODELING

The suitable and accurate designs of the wire condenser help the system to work in a good situation and decrease the power consumption, but on another side, it means an acceptable cost. The following assumptions are considered in the modeling of the wire-on-tube condenser: steady-state case and one-dimensional analysis, and cross-flow heat exchanger, unmixed refrigerant side and mixed airside. The bends affect heat transfer. The saturated (two-phase) region for the refrigerant is considered homogenous mixture. Properties of the refrigerants are uniform thermodynamically. There is no change in the temperature and pressure of the refrigerant with the radius of the tube. **Muller-Stenhagan, and Heck, 1986** correlations were used to calculate the fraction pressure drop in the two-phase flow. **Domanski, and Hermes, 2008** correlations were be used to calculate the bends pressure drop in the two-phase flow. The thermodynamic model for a wire condenser is done according to the two methods of calculation: Zones method and Integral method.

3.1 Zones Method

This method is done by dividing the condenser into the regions according to the process and phase change, which is a single or two-phase flow. Also, the suitable equations are used to calculate the heat transfer coefficient and pressure drop for each region. The wire tube condenser is divided into the refrigerant side and the air side. The refrigerant side has three regions: superheat, two-phase flow, and subcooled.

3.1.1 The superheat region

It's the first part of the condenser and the refrigerant in the gas phase. The heat transfer coefficient can be determined according to Dittus-Boelter correlation from reference **Holman, 2010**:

$$Nu = 0.023 * Re_g^{0.8} * Pr^{0.3} \tag{1}$$

Where: $Nu = \frac{\propto_{supeeheat} * Dt_i}{k_g}$

The properties are evaluated at the film temperature, T_{film}.

$$T_{film} = \frac{T_{wall} + T_{bulk}}{2} \tag{2}$$

Where: $Re_g = \frac{G * Dt_i}{\mu_g}$

The heat rejected is given by:

$$Q_{super\ heat} = \dot{m}_r cp * (T_{in} - T_{cin-sat}) \tag{3}$$

$$Q_{super\ heat} = \alpha_{superheat} A_{si} * \left(\frac{T_{in} - T_{wi}}{2}\right) \tag{4}$$

Where: $A_{si} = \pi \cdot Dt_i \cdot L_{superheat}$

T_{in}= The inlet temperature to superheat region.

$T_{cin-sat}$ =The inlet temperature to saturated region.
T_{wi} = The temperature of the inner tube wall.
The total pressure drop is the summation of the friction pressure drop, momentum pressure drop, and bending pressure drop as well as the gravity pressure drop for the vertical tube only. The friction pressure drop is calculated by the Darcy equation, **Bruce, and Donald, 2002:**

$$\Delta P_{friction} = 2 \cdot f_g \cdot \frac{L_{superheat}}{Dt_i} \cdot \frac{G^2}{\rho_{in}} \quad (5)$$

The friction factors are given by **Dobson, 1994**:

$$f_g = 0.046 * Re_g{}^{-0.2} \quad (6)$$

The momentum pressure drop is calculated from reference **Traviss, 1972**:

$$\Delta P_{mom} = \frac{-G^2 - \left(\frac{1}{\rho_{out}} - -\frac{1}{\rho_{in}}\right)}{L_{superheat}} \quad (7)$$

The bending pressure drop is calculated from reference **Bruce, and Donald, 2002**:

$$\Delta P_{bends} = f_g * \frac{G^2}{2.\rho_{in}} * \frac{L_{bend}}{Dt_i} * N_{bends} \quad (8)$$

Where: $L_{bend} = \frac{\pi * p_t}{2}$, N_{bends} is the number of bends, and p_t is the bend length.
The gravity pressure drop is the change due to the elevations of the discharge tube. This is calculated from hydrostatics:

$$\Delta P_{gravity} = \rho_g * g * L_{discharge} \quad (9)$$

3.1.2 The two-phase region
It's the second part of the condenser, which covers the largest part of the total area of the condenser. The first step is to find the type of flow pattern to calculate the heat transfer coefficient, the two-phase flow may be stratified, stratified-wavy, annular, intermitted, and mist flow, shown in **Fig. 2**.

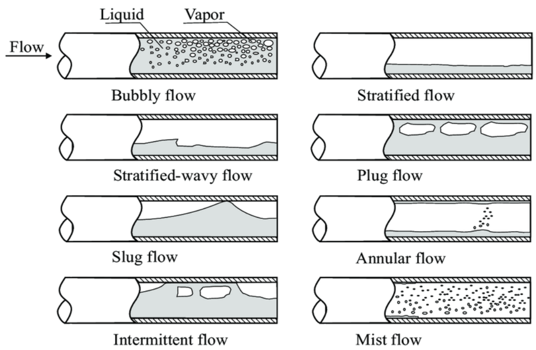

Figure 2. The flow pattern types.

The logarithmic mean void fraction will be used to calculate the flow pattern regions according to, **Hajal, 2003:**
The void fraction is:

$$\varepsilon = \frac{\varepsilon_h - \varepsilon_{ra}}{\ln\left(\frac{\varepsilon_h}{\varepsilon_{ra}}\right)} \quad (10)$$

The homogeneous void fraction is:

$$\varepsilon_h = \left[1 + \left(\frac{1-x}{x}\right)\left(\frac{\rho_V}{\rho_L}\right)\right]^{-1} \quad (11)$$

The Rouhani-Axelsson void fraction is:

$$\varepsilon_{ra} = \frac{x}{\rho_V}\left([1 + 0.12(1-x)]\left[\frac{x}{\rho_V} + \frac{1-x}{\rho_L}\right] + \frac{1.18(1-x)[9.81 * \sigma(\rho_l - \rho_v)]^{0.25}}{G\rho_L^{0.5}}\right)^{-1} \quad (12)$$

The liquid film Reynold number is:

$$Re_L = \frac{4G(1-x)\delta}{(1-\varepsilon)\mu_L} \; or \; \frac{GDt_i(1-x)}{\mu_L} \tag{13}$$

Fig. 3 shows the geometrical dimensions of a stratified flow where: $p_L$is the stratified perimeter around the bottom of the tube. p_V is the non-stratified perimeter around the top of the tube. h_L is the height of the stratified liquid. p_i is the length of the interface.A_L and A_V are the corresponding cross-sectional areas occupied by the liquid and vapor. Four of these dimensions would be found using the internal diameter of the tube.

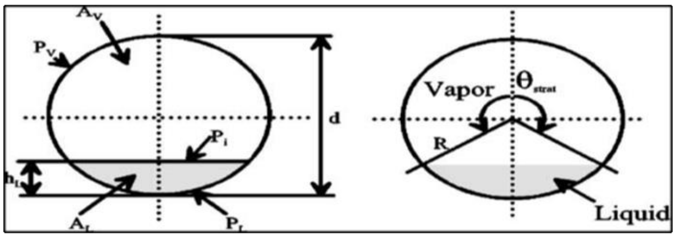

Figure 3. The geometrical parameters for two-phase flow in a circular tube.

$$h_{Ld} = \frac{h_L}{Dt_i}, P_{id} = \frac{P_i}{Dt_i}, A_{Ld} = \frac{A_L}{Dt_i^2}, A_{Vd} = \frac{A_V}{Dt_i^2} \tag{14}$$

The cross-sectional area occupied by liquid and vapor, **Hajal, 2003**:

$$A_L = A(1-\varepsilon) \tag{15}$$

$$A_V = A\varepsilon \tag{16}$$

The dimensionless liquid cross sectional area, **Hajal, 2003**:

$$A_{Ld} = \frac{1}{8}[(2\pi - \theta_{strat}) - \sin(2\pi - \theta_{strat})] \tag{17}$$

The dimensionless liquid height:

$$h_{Ld} = 0.5\left(1 - \cos\left(\frac{2\pi - \theta_{strat}}{2}\right)\right) \tag{18}$$

The dimensionless perimeter of interface, **Hajal, 2003**:

$$P_{id} = \sin\left(\frac{2\pi - \theta_{strat}}{2}\right) \tag{19}$$

The stratified angle around the upper perimeter of the tube:

$$\theta_{strat} = 2\pi - 2\left\{\pi(1-\varepsilon) + \left(\frac{3\pi}{2}\right)^{1/3}\left[1 - 2(1-\varepsilon) + (1-\varepsilon)^{\frac{1}{3}} - \varepsilon^{1/3}\right] - \frac{1}{200}(1-\varepsilon)\varepsilon[1 - 2(1-\varepsilon)][1 + 4((1-\varepsilon)^2 + \varepsilon^2)]\right\} \tag{20}$$

The mass velocity of the wavy flow, **Hajal, 2003**:

$$G_{wavy} = \left\{\frac{16A_{Vd}^3 * 9.81 * Dc_i\rho_L\rho_V}{x^2\pi^2(1-(2h_{Ld}-1)^2)^{0.5}}\left[\frac{\pi^2}{25h_{Ld}^2} * \left(\frac{We}{Fr}\right)_L^{-1.023} + 1\right]\right\}^{0.5} + 50 - 75e^{-\left(x^2-0.97\right)^2/x(1-x)} \tag{21}$$

The mass velocity of the stratified flow, **Hajal, 2003**:

$$G_{strat} = \left\{\frac{(226.3)^2 A_{Ld}A_{Vd}^2\rho_V(\rho_L-\rho_V)\mu_L * 9.81}{x^2(1-x)\pi^3}\right\}^{1/3} + 20x \tag{22}$$

The vapor quality at the transition from intermittent to annular flow, **Hajal, 2003**:

$$x_{IA} = \left\{\left[0.2914\left(\frac{\rho_V}{\rho_L}\right)^{-1/1.75}\left(\frac{\mu_L}{\mu_V}\right)^{-1/7}\right] + 1\right\}^{-1} \tag{23}$$

The ratio of the liquid Weber number to the liquid Froude number, **Hajal, 2003**:

$$\left(\frac{We}{Fr}\right)_L = \frac{9.81 * Dt_i^2\rho_L}{\sigma} \tag{24}$$

The factor ξ, **Hajal, 2003**:

$$\xi = \left[1.138 + 2\log\left(\frac{\pi}{1.5A_{Ld}}\right)\right]^{-2} \tag{25}$$

The mass velocity of the mist flow, **Hajal, 2003**:

$$G_{mist} = \left\{\frac{7680A_{Vd}^2 * 9.81 * Dt_i\rho_L\rho_V}{x^2\pi^2\xi}\left(\frac{Fr}{We}\right)_L\right\}^{0.5} \tag{26}$$

The mass velocity of the bubbly flow, **Hajal, 2003**:

$$G_{bubbly} = \left\{\frac{256A_{Vd}^{2}Dt_i^{1.25}\rho_L(\rho_L-\rho_V)*9.81}{0.3164(1-x)^{1.75}\pi^2 P_{id}\mu_L^{0.25}}\right\}^{1/1.75} \quad (27)$$

To identify the flow pattern at a particular value of vapor quality x, the following limitations are to be applied**, Hajal, 2003**:

- Annular flow exists if $G > G_{wavy}$, $G < G_{mist}$ $and\ x > x_{IA}$.
- Intermittent flow exists if $G > G_{wavy}$ and $G < G_{mist}$ or $G < G_{bubbly}$ $and\ x < x_{IA}$.
- Stratified-wavy flow exists if $G_{strat} < G < G_{wavy}$;
- Fully stratified flows exist if $G < G_{strat}$.
- Mist flow exists if $G > G_{mist}$.

Three procedures can calculate the heat transfer coefficient according to the flow pattern type**.**

If the flow pattern is stratified-wavy, then the heat transfer coefficients are calculated from **Hajal, 2003**:

$$\alpha_{tp} = \frac{\alpha_f*\frac{Dt_i}{2}*\theta+[2*\pi-\theta]*\frac{Dt_i}{2}*\alpha_c}{2*\pi*\frac{Dt_i}{2}} \quad (28)$$

The upper angle of the tube not wetted by stratified liquid:

$$\theta = \theta_{strat}\left[\frac{(G_{wavy}-G)}{(G_{wavy}-G_{strat})}\right]^{0.5} \quad (29)$$

The convective condensation heat transfer coefficient:

$$\alpha_c = c*Re_l^n*Pr_l^m*\frac{k_l}{\delta_{lW}}*f_i \quad (30)$$

Where:$c = 0.003, n = 0.74$ and $m = 0.5$ from **Hajal, 2003**:

$$f_i = 1+\left[\frac{u_v}{u_l}\right]^{0.5}*\left[\frac{(\rho_l-\rho_g)*9.81*\delta_{lW}^2}{\sigma}\right]^{0.25} \quad (31)$$

The liquid film thickness flow for the stratified-wavy **Hajal, 2003**:

$$\delta_{lW} = \frac{Dt_i-\left[Dt_i^2-A_l*\frac{8}{2\pi-\theta}\right]^{0.5}}{2} \quad (32)$$

The Nusselt film condensing coefficient on the top perimeter of the tube according to:

$$\alpha_f = 0.728*\left[\frac{\rho_l*(\rho_l-\rho_g)*9.81*h_{fg}*k_l^3}{\mu_l*Dc_i*\Delta T}\right]^{0.25} \quad (33)$$

$h_{fg} = J/kg$, $\Delta T = T_{sat} - T_w$

If the flow is fully stratified, then the heat transfer coefficients calculate from:

$$\alpha_{tp} = \frac{\alpha_f*\frac{Dt_i}{2}*\theta_{strat}+[2*\pi-\theta_{strat}]*\frac{Dt_i}{2}*\alpha_c}{2*\pi*\frac{Dt_i}{2}} \quad (34)$$

The convective condensation heat transfer coefficient:

$$\alpha_c = c*Re_l^n*Pr_l^m*\frac{k_l}{\delta_{lS}}*f_i \quad (35)$$

Where:$c = 0.003, n = 0.74$ and $m = 0.5$ from **Hajal, 2003**

$$f_i = 1+\left[\frac{u_v}{u_l}\right]^{0.5}*\left[\frac{(\rho_l-\rho_g)*9.81*\delta_{lS}^2}{\sigma}\right]^{0.25}\left(\frac{G}{G_{strat}}\right) \quad (36)$$

The liquid film thickness flow for the fully-stratified:

$$\delta_{lS} = \frac{Dt_i-\left[Dt_i^2-A_l*\frac{8}{2\pi-\theta_{strat}}\right]^{0.5}}{2} \quad (37)$$

The important point is the length of the two-phase area; with an inner diameter of 4.42mm and 3.25mm, so the area is the target. The approximate length can be found from the relation of the energy balance:

$$Q_{two-phase} = \dot{m}_r*h_{fg} \quad (38)$$

$$\alpha_{tp}*A_{s-tp}*\Delta T = \dot{m}_r*h_{fg}*\Delta x \quad (39)$$

$G = \frac{\dot{m}_r}{A_c}$, and $A_c = \pi * Dt_i^2/4$

$\alpha_{tp} * \pi * Dt_i * l * \Delta T = G * \frac{\pi * Dt_i^2}{4} * h_{fg} * \Delta x$

Let $l = dz \ and \ \Delta x = dx$

Re-arrangement yield:

$\frac{dz}{dx} = \frac{G * h_{fg} * Dt_i}{4 * \alpha_{tp} * \Delta T}$

$\int dz = \frac{G * h_{fg} * d_i}{4 * \alpha_{tp} * \Delta T} \int dx$

It is the length of the tube required to cover the change in the quality, and the average heat transfer coefficient can be found from the following:

$\frac{1}{\alpha_{tp}} = \frac{1}{x_i - x_e} \int_{xe}^{xi} \frac{dx}{dz}$ This expression is a function for quality only.

$$Q_{two-phase} = \alpha_{tp} \cdot A_{i-tp} \cdot (T_R - T_{win}) \quad (40)$$

Where: $A_{i-tp} = \pi * Dt_i * L_{tp}$

The total pressure drop in the saturated region is the summation of pressure drop due to, friction, momentum. The gravity pressure drop is the horizontal layout of the tubes will be neglected, according to **ASHRAE, 1997**.

$$\Delta P_{tp-total} = \Delta P_{tp-friction} + \Delta P_{tp-mom} + \Delta P_{tp-bends} \quad (41)$$

The friction pressure drop is calculated using Müller-Steinhagen and Heck correlation according to **ASHRAE, 1997**:

$$\left(\frac{dp}{dz}\right)_{tp-friction} = \Lambda \cdot (1-x)^{\frac{1}{3}} + \left(\frac{dp}{dz}\right)_{lo} \cdot x^3 \quad (42)$$

$$\Lambda = \left(\frac{dp}{dz}\right)_{lo} + 2 \cdot \left[\left(\frac{dp}{dz}\right)_{go} - \left(\frac{dp}{dz}\right)_{lo}\right] \cdot x \quad (43)$$

Where: $\left(\frac{dp}{dz}\right)_{lo} = f_l \cdot \frac{2 \cdot G_{tot}^2}{D_i \cdot \rho_l}$, $\left(\frac{dp}{dz}\right)_{go} = f_g \cdot \frac{2 \cdot G_{tot}^2}{D_i \cdot \rho_g}$, $f = 0.079 * Re^{-0.25}$ and $Re = \frac{G_{tot} \cdot D_i}{\mu}$

The momentum pressure drop calculated from **ASHRAE, 1997**:

$$\frac{dp}{dz_{mom}} = -G^2 \cdot \frac{d}{dz}\left\{\frac{x^2}{\rho_g \cdot \varepsilon_{zivic}} + \frac{(1-x^2)}{\rho_l \cdot (1-\varepsilon_{zivic})}\right\} \quad (44)$$

Where ε is the void fraction for Zivic:

$$\varepsilon_{zivic} = \left[1 + \left(\frac{1-x}{x}\right)\left(\frac{\rho_g}{\rho_l}\right)^{0.67}\right]^{-1} \quad (45)$$

The final form used to calculate the momentum pressure drop is:

$$\Delta P_{tp-mom} = G^2 - \left\{\left[\frac{x^2}{\rho_g \cdot \varepsilon_{zivic}} + \frac{(1-x)^2}{\rho_l \cdot (1-\varepsilon_{zivic})}\right]_2 - \left[\frac{x^2}{\rho_g \cdot \varepsilon_{zivic}} + \frac{(1-x)^2}{\rho_l \cdot (1-\varepsilon_{zivic})}\right]_1\right\} \quad (46)$$

Bending pressure drop**: Domanski, 2008** proposed a new correlation based on the two-phase friction pressure drop correlation for straight tubes by Müller- Steinhagen and Heck Correlation and a multiplier to accounts for the bend curvature.

$$\Delta P_{tp-bend} = 0.0065 \cdot \left(\frac{G \cdot D \cdot x}{\mu_g}\right)^{0.54} \cdot \left(\frac{1}{x} - 1\right)^{0.21} \cdot \left(\frac{\rho_l}{\rho_g}\right)^{0.34} \cdot \left(\frac{2R}{d_i}\right)^{-0.67} \cdot \Delta P_{tp-st} \quad (47)$$

The total pressure drop for bends is:

$$\Delta P_{tp-bends} = \sum \Delta P_{tp-bend} \quad (48)$$

3.1.3 The subcooled region:

It's the last part of the condenser and the refrigerant in the liquid phase. The heat transfer coefficient and pressure drop are the same as the superheat region.

3.1.4 Final calculation:

To find the total length for condenser:

$$L_c = L_{superheat} + L_{tp} + L_{subcooled} \quad (49)$$

The average heat transfer coefficient is:

$$\alpha_{ic} = \frac{(L_{superheat}*\alpha_{superh})+(L_{tp}*\alpha_{avetp})+(L_{subcooled}*\alpha_{subcooled})}{L_c} \quad (50)$$

3.1.5 Airside:

The condenser shape and configuration allow a good understanding of the behaviors of the heat transfer and the pressure drop. Before clarifying the analysis of the condenser airside, the fin efficiency, the finned tube surface effectiveness, the overall heat transfer coefficient, and the Ɛ-NTU method should be determined as follows:

The actual fin efficiency is calculated using the approximation for fin geometry relation **Holman, 2010**:

$$\eta_f = \frac{tanh(m_{fin} \cdot L_{fin})}{m_{fin} \cdot L_{fin}} \quad (51)$$

Where: $m_{fin} = \sqrt{\frac{4\cdot(\alpha_{cav}+\alpha_{crad})}{K_{fin}\cdot D_f}}$, α_{air} is the heat transfer coefficient of air.

K_{fin} is the thermal conductivity of the fin. D_f is the diameter of the wire fin.

The finned tube surface is described using its areas, where:

$$A_{tot} = A_f + A_{tube} \quad (52)$$

$$A_f = \pi * D_f * L_f * No.fins - A_{contact} \quad (53)$$

$$A_{tube} = (\pi * D_{to} * L_c - A_{contact}) \quad (54)$$

$$A_{contact} = \left(D_f * D_{to} * 0.75\right) * No.legs * No.fins \quad (55)$$

The heat transfer coefficient for horizontal surfaces (tubes) α_{cah} equations, **Holman, 2010:**

$$Ra_h = \frac{9.81*\beta*[T_{cs}-T_{amb}]*Dc_o^3*Pr_a}{\nu^2} \quad (56)$$

If $[Ra_h < 10^9]$

$$\alpha_{cah} = 1.32 * \left[\frac{T_{cs}-T_{amb}}{Dc_o}\right]^{0.25} \quad (57)$$

If $[Ra_h > 10^9]$

$$\alpha_{cah} = 1.52 * [T_{cs} - T_{amb}]^{0.3333} \quad (58)$$

The heat transfer coefficient for vertical surfaces (fins) is α_{cav} equations, **Holman, 2010:**

$$Ra_h = \frac{9.81*\beta*[T_{cs}-T_{amb}]*H_c^3*Pr_a}{\nu^2} \quad (59)$$

If $[Ra_h < 10^9]$

$$\alpha_{cav} = 1.42 * \left[\frac{T_{cs}-T_{amb}}{H_c}\right]^{0.25} \quad (60)$$

If $[Ra_h > 10^9]$

$$\alpha_{cav} = 1.31 * [T_{cs} - T_{amb}]^{0.3333} \quad (61)$$

The radiation heat transfer coefficient α_{crad}, **Holman, 2010:**

$$\alpha_{crad} = \epsilon * 5.67 * 10^{-8} * \left[\frac{(T_{cs})^4-(T_{amb})^4}{T_{cs}-T_{amb}}\right] \quad (62)$$

To calculate the surface efficiency:

$$\eta_s = 1 - \frac{A_{fin}}{A_{tot}}\left(1 - \eta_{fin}\right) \quad (63)$$

The heat transfer from the wire condenser, **Holman, 2010:**

$$Q_{fin} = [\alpha_{cav} + \alpha_{crad}] * A_f * [T_{cs} - T_{amb}] * \eta_{fin} \quad (64)$$

$$Q_{tube} = [\alpha_{cah} + \alpha_{crad}] * A_{tube} * [T_{cs} - T_{amb}] \quad (65)$$

$$Q_{c-a\,total} = Q_{fin} + Q_{tube} \quad (66)$$

$$R_{oc} = \frac{1}{[\alpha_{cah}+\alpha_{crad}]*A_{tot}*\eta_s} \quad (67)$$

$$R_{ic} = \frac{1}{\alpha_{ic}*A_i} \quad (68)$$

The overall heat transfer coefficient is determined by the following equation**, Holman, 2010:**

$$\frac{1}{UA} = \frac{1}{\eta_s \cdot \alpha_{ac} \cdot A_{tot}} + \frac{\ln \frac{r_o}{r_i}}{2\pi . K_p . L_c} + \frac{1}{\alpha_{ic} \cdot A_i} \qquad (69)$$

The effect of fouling inside and outside is neglected because the refrigerator is brand new.
The effectiveness of the wire condenser is calculated by assumption the heat exchanger unmixed-mixed and cross-flow configuration, **Holman, 2010**:

$$\mathcal{E}_{H.E} = 1 - \exp\{-(1/C^*) \cdot [1 - exp(-NTU \cdot C^*)]\} \qquad (70)$$

Where: $C^* = \frac{C_{min}}{C_{max}}$ and $C = \dot{m} * C_p$

Also $\mathcal{E}_{H.E}$ can be defined as:

$$\mathcal{E}_{H.E} = \frac{Q_{act}}{Q_{max}} = \frac{\dot{m} \cdot C_{min} \cdot (T_{ci} - T_{co})}{\dot{m} \cdot C_{min} \cdot (T_{hi} - T_{ci})} \qquad (71)$$

This leads to:

$$\mathcal{E}_{H.E} = \frac{(T_{ci} - T_{co})}{(T_{hi} - T_{ci})} \qquad (72)$$

$$NTU = \frac{UA}{C_{min}} \qquad (73)$$

3.2 Integral Method:

The integral method was done according to **Ragazzi, and Pedersen, 1991,** for the saturated region only by dividing this region to elements and calculate the heat transfer coefficient and pressure drop by integrating. This method was done by integrating the equations that depend on dryness friction of refrigerant from 0.95 to 0.05. In this method, the parameter can be analyzed and find when the flow pattern changes from stratified-wavy flow to fully-stratified flow. Also, the heat transfer coefficient and pressure drop can be found locally according to dryness friction percent. In this method, an integral solution was used to find the heat transfer coefficient. The equations and the procedure are the same as the two-phase region in zones method but with integral according to the dryness friction.

3.3 Exergy Analysis of the Condenser:

The condenser represents the second component in the vapor compression refrigeration system. The condenser is made of iron tube and fins are painted with black color, according to **Bejan, 1996**:
The energy:

$$\dot{m}_r \cdot h_4 + \dot{m}_a \cdot h_{ainc} = \dot{m}_r \cdot h_5 + \dot{m}_a \cdot h_{aoutc} + Q_{cond\ losses} \qquad (74)$$

$$Q_{cond\ losses} = \dot{m}_r \cdot (h_4 - h_5) + \dot{m}_a \cdot (h_{ainc} - h_{aoutc}) \qquad (75)$$

The exergy analysis:

$$ED_{cond} = \left(1 - \frac{T_{amb}}{T_{wallcond}}\right) Q_{cond\ losses} + \sum_{in} ex - \sum_{out} ex \qquad (76)$$

Where:

$$\sum_{in} ex = \dot{m}_r \cdot \left(ex_4 + \frac{P_{4rcond}}{\rho_4}\right) + \dot{m}_a \cdot \left(ex_{ainc} + \frac{P_{ainc}}{\rho_{ain}}\right)$$

$$\sum_{out} ex = \dot{m}_r \cdot \left(ex_5 + \frac{P_{5rcond}}{\rho_5}\right) + \dot{m}_a \cdot \left(ex_{aoutc} + \frac{P_{aoutc}}{\rho_{aout}}\right)$$

$$ex_4 = (h_4 - h_o) - T_o \cdot (s_4 - s_o)$$

$$ex_5 = (h_5 - h_o) - T_o \cdot (s_5 - s_o)$$

$$ex_{ainc} = (h_{ainc} - h_o) - T_o \cdot (s_{ainc} - s_o)$$

$$ex_{aoutc} = (h_{aoutc} - h_o) - T_o \cdot (s_{aoutc} - s_o)$$

The final form for the exergy analysis is:

$$ED_{cond} = \left(1 - \frac{T_o}{T_{wallcond}}\right) Q_{lossescond} + \dot{m}_r \cdot \left[(ex_4 - ex_5) + \frac{\Delta P_{45cond}}{\rho_4}\right] + \dot{m}_a \cdot (ex_{ainc} - ex_{aoutc}) \qquad (77)$$

$$\zeta_{cond} = \frac{ED_{cond}}{Power_{total}} \qquad (78)$$

The exergy efficiency is given by:

$$\eta_{cond} = 1 - \zeta_{cond} \qquad (79)$$

3.4 Optimum Tube Diameter of the Condenser:

The optimum diameter of tube condenser is divided into two cases; the first is internal flow optimization, and the second is external flow optimization.

3.4.1 Internal flow optimization:

The optimum size of the internal tube diameter of the condenser is found according to Entropy-Generation Minimization from **Bejan, 2006**. This theory is based on the relation between the entropy generation number and the Reynolds number.

The entropy generation number is calculated from:

$$N_s = \frac{\dot{S}_{gen}}{\dot{S}_{gen,min}} = 0.856 * \left(\frac{Re}{Re_{opt}}\right)^{-0.8} + 0.144 * \left(\frac{Re}{Re_{opt}}\right)^{4.8} \quad (80)$$

The optimum Reynolds number is calculated from:

$$Re_{opt} = 2.023 * Pr^{-0.071} * B_o^{0.358} \quad (81)$$

The Parameter B_o calculated from:

$$B_o = \dot{m} * q' * \frac{\rho}{\mu^{5/2} * (k_f * T_{sat})^{0.5}} \quad (82)$$

The Reynolds number: $Re = \frac{4 * \dot{m}}{\pi * Dt_i * \mu_l}$ (83)

3.4.2 External flow optimization:

The optimum size of the external tube diameter of the condenser is found according to Entropy-Generation Minimization theoretical analysis for external flow around the horizontal cylinder at low Reynolds number from **Mahdi, 2018**. This theory depends on the relation between the entropy generation number and Reynolds number ratio, which is calculated from:

$$N_{s1} = \frac{\dot{S}_{gen}}{\dot{S}_{gen,min}} = \left(\frac{Re}{Re_{opt}}\right)^{-0.33} + \left(\frac{Re}{Re_{opt}}\right)^{0.216} \quad (84)$$

$$N_{s2} = \frac{\dot{S}_{gen}}{\dot{S}_{gen,min}} = \left(\frac{Re}{Re_{opt}}\right)^{-0.385} + \left(\frac{Re}{Re_{opt}}\right)^{0.698} \quad (85)$$

$$N_{s3} = \frac{\dot{S}_{gen}}{\dot{S}_{gen,min}} = \left(\frac{Re}{Re_{opt}}\right)^{-0.466} + \left(\frac{Re}{Re_{opt}}\right)^{0.8} \quad (86)$$

$$N_{s4} = \frac{\dot{S}_{gen}}{\dot{S}_{gen,min}} = \left(\frac{Re}{Re_{opt}}\right)^{-0.618} + \left(\frac{Re}{Re_{opt}}\right) \quad (87)$$

Equations are used according to the range of Reynolds number (Re):

If 0.4 < Re < 4 then use equation (84) and the optimum Reynolds number is calculated from:

$$Re_{opt} = 0.139 * {\beta_0}^{1/0.546} \quad (88)$$

If 4 < Re < 40 then use equation (85) and the optimum Reynolds number is calculated from:

$$Re_{opt} = 0.722 * {\beta_0}^{1/1.083} \quad (89)$$

If 40 < Re < 4000 then use equation (86) and the optimum Reynolds number is calculated from:

$$Re_{opt} = 1.824 * {\beta_0}^{1/1.266} \quad (90)$$

If 4000 < Re < 40000 then use equation (87) and the optimum Reynolds number is calculated from:

$$Re_{opt} = 14.64 * {\beta_0}^{1/1.618} \quad (91)$$

Where $Re = \frac{\rho_\infty U_\infty Dt_o}{\mu_\infty}$

Where β_0 is the duty parameter calculated from:

$$\beta_0 = \frac{{q'}^2}{U_\infty^2 k_\infty \mu_\infty T_\infty Pr^{1/3}} \quad (92)$$

The analysis and the optimization of the condenser were carried out using EES software.

5. RESULTS AND DISCUSSION:

The experimental work done for four cases is given in **Table (1)**:

Figs. 4 and 5 show the T-s and P-h diagrams of the vapor compression refrigeration cycle with R-134a as a working fluid for two condensers with different diameters 6.35 mm and 4.76 mm at 32˚C ambient temperature. The compression ratio remained constant, which means that the compression ratio was not affected by the change of condenser tube diameter. The condenser and evaporator pressures and temperatures decrease with the increase in the condenser tube diameter because the subcooled region was increased. The dryness fraction at the evaporator inlet decreases with the increase in the condenser tube diameter, which gives a better cooling effect in the evaporator. The maximum and minimum temperatures of each cycle are shifted up with the decrease in the condenser tube diameter due to the pressure drop, which increases at small diameter.

Table 1. Table of all the tests.

No.	Diameter(mm)	Refrigerant type	Test No.	Charge (g)	Tevp ℃	Time (min)
1	4.76 (3/16")	R-134a	1	60g	-18	150 min
			2	70g	-22	135 min (optimum)
			3	80g	-19	160 min
2	6.35 (1/4")	R-134a	1	80g	-15	120 min
			2	100g	-22	90 min (optimum)
			3	120g	-16	130 min
3	4.76 (3/16")	R-600a	1	20g	-17	120 min
			2	30g	-22	90 min (optimum)
			3	40g	-15	130 min
4	6.35 (1/4")	R-600a	1	30g	-15	120 min
			2	50g	-23	90 min (optimum)
			3	70g	-18	120 min

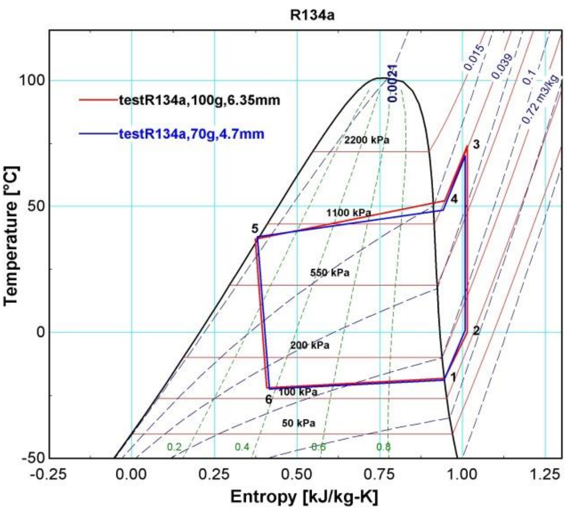

Figure 4. The P-h diagram of vapor compression refrigeration cycle with R-134a and different tube diameter of condensers.

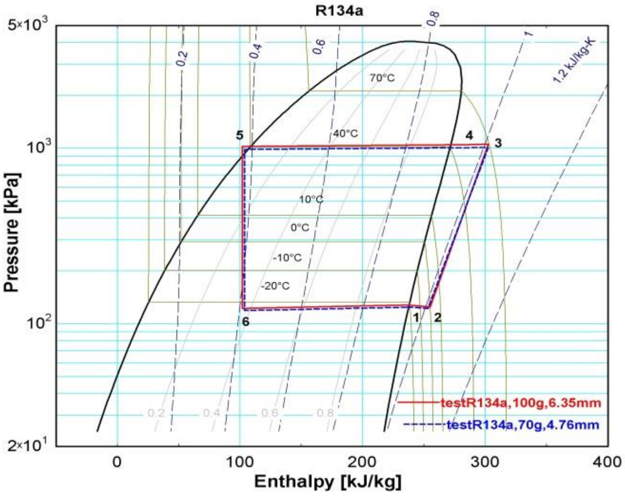

Figure 5. The T-s diagram of vapor compression refrigeration cycle with R-134a and different tube diameter of

Figs. 6 and 7 depict the T-s and P-h diagrams of the vapor compression refrigeration cycle with R-600a as a working fluid for two condensers with different diameters 6.35 mm and 4.76 mm at 32˚C ambient temperature. The compression ratio is not constant, because the change in the tube diameter of condenser affected the flow stream in the tube because the density of R-600a is greater than R-134a and mass inventory for the large tube is higher than the small tube. The condenser and evaporator pressures and temperatures decrease with the increase in the condenser tube diameter because of the same reason given above. The dryness fraction decreases with the increase in the condenser tube diameter, which gives a better cooling effect in the evaporator. The maximum and minimum temperatures of each cycle are also shifted up with the increase in the condenser tube diameter.

Fig. 8 depicts the heat transfer coefficient for the refrigerant side in the superheat region, the two-phase flow region, and subcooled region, in the condenser for four tests. This figure shows that the average heat transfer of the refrigerant R-600a is higher than the refrigerant R-134a for all tests. This happens due to the high turbulence in the refrigerant flow. The heat transfer coefficient in the subcooled is the lowest for all tests, and the heat transfer coefficient of the two-phase region is the highest for all tests because the tube for the two-phase flow is longer than the other regions.

Fig. 9 demonstrates the total pressure drop in the condenser for the superheat region, two-phase flow region, subcooled region, and the total condenser. This figure shows that the pressure drop in the condenser of the refrigerant R-600a is higher than the refrigerant R-134a for all tests because the density of R-600a is higher and the properties for R-600a is different for R134a. Also, the pressure drop in the condenser with 4.76 mm tube diameter is higher than the condenser with 6.35 mm tube diameter for all tests, because the velocity is higher in the small diameter.

Figs. 10, 11, and 12 clarify the pressure drop in the condenser due to the friction, momentum, and bends for all zones. These figures show that the pressure drop in the condenser working with the refrigerant R-600a is higher than the condenser working with refrigerant R-134a for all tests because the density is higher and the properties for R-600a is different for R134a. Also, the pressure drop in the condenser with a 4.76 mm tube diameter is higher than the condenser with 6.35 mm tube diameter for all tests due to the high turbulence of refrigerant flow.

Fig. 13 indicates the exergy efficiency of the condenser for tests 1, 2, 3, and 4 is 93.96%, 92.32%, 88.46%, and 87.14%, respectively, it is concluded that for the same refrigerant, the exergy efficiency of condenser with tube diameter 4.76 mm is smaller than the condenser with tube diameter 6.35 mm because the pressure drop is higher. And, for the same tube diameter of condenser, the exergy efficiency of condenser working with R-600a is smaller than the condenser working with R-134a because the heat losses are higher.

Fig. 14 reveals the C.O.P for all tests compared with C.O.P for cycle Carnot. This figure shows the performance of the system, which usually looks where the Carnot is higher than the actual test three times.

Fig. 15 elucidates the second law thermodynamic efficiency for all tests. This figure shows that the test four (R-600a, 4.76 mm) has higher thermodynamical efficiency than the other.

Fig. 16 reveals the calculated total length of condenser required to remove the heat from the refrigerant to ambient, and show the length of the necessary condenser for all zones. This figure explains that the total length of condenser working with R-134a is greater than the actual length, but the total length of condenser working with R-600a is lower than the actual length, because the heat transfer coefficient of the refrigerant R-600a is greater than the refrigerant R-134a.

Fig. 17 depicts the optimum diameter for the outer conditions of the condenser. All tests are located on the heat dominated region because in the natural convection, the losses due to the friction are very low, and most of these losses are due to the heat. The nearest test on the optimum point is the test (R-134a, 6.35 mm) because the outer area is larger than the other.

Fig. 18 reveals the optimum diameter for the inside tube of the condenser. The condenser of test one

(R-134a, 6.35 mm) is located on the friction dominated region nearly the optimum point, and the condenser of test two (R-134a, 4.76 mm) is located on the friction dominated region, also far away from the optimum point, because the friction losses in the condensers are dominated. Also, this figure shows that test three (R-600a, 6.35 mm) and four (R-600a, 4.76 mm) are located on the heat dominated region apart from the optimum point because the heat losses are dominated. Test four (R-600a, 4.76 mm) is the closed test to the optimum point as referred before in the exergy efficiency section and the best.

Fig. 19 manifests the distribution of heat transfer coefficient with the dryness fraction by the integral method. The heat transfer coefficient of the test (R-600a, 4.76 mm) is greater than other tests, but the heat transfer coefficient of the test (R-134a, 6.35 mm) is lower than other tests, which are identical to the zone method.

Figs. 20, 21, and 22 displays the distribution of the friction, momentum, and total pressure drop in the condenser with dryness fraction. These figures show the pressure drop of the tests with a 4.76 mm tube diameter is higher than the other tests, which also agrees with the total zones method.

Fig. 23 demonstrates the total length of condenser distribution with a dryness fraction. This figure shows that the tests working with R-134a are higher than the other tests due to the difference in the heat transfer coefficient.

Fig. 24 shows the comparison between the two methods of calculating the length: zone method and integral method. There is a different length calculated by two methods. The difference is 10% between the two methods, and the integral method gives the longer condenser.

Fig. 25 shows a comparison between the two methods of calculating the heat transfer coefficient. The zone method produces lower average heat transfer coefficient by 11% than the integral method integral.

Fig. 26 exhibits the total pressure drop difference; also, the integral method is higher than the zone method by 20%.

Fig. 27 indicates that the pressure drop in the experimental tests is higher than the pressure drop calculated in the two methods because the result of the two methods is calculated for the pure refrigerant, but in fact, the refrigerant is not pure. Also, the friction pressure drop in the bends is higher than the pressure drop calculated from the two methods caused by the errors of instrumentation and variable input data.

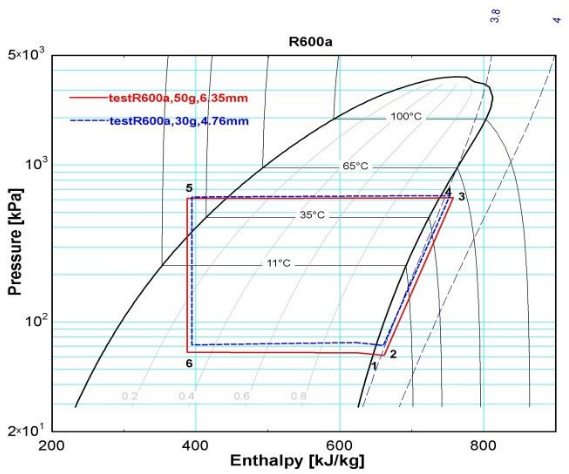

Figure 6. The P-h diagram of vapor compression refrigeration cycle with R-600a and different tube diameter of condensers.

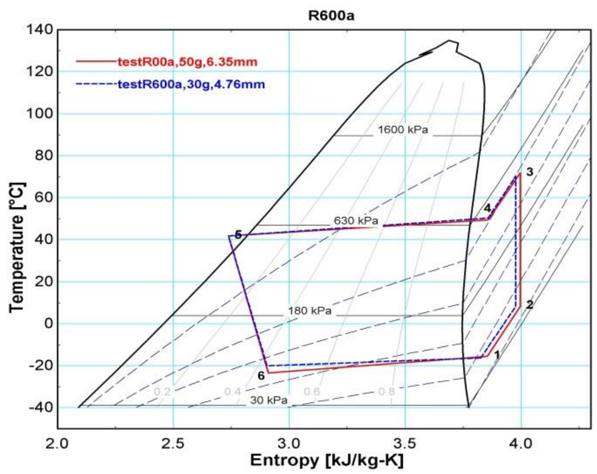

Figure 7. The T-s diagram of vapor compression refrigeration cycle with R-600a and different tube diameter of condensers.

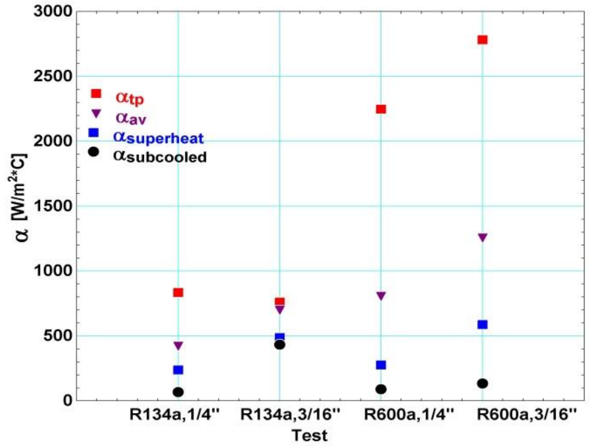

Figure 8. Heat transfer coefficient for all zones in condenser with the tests.

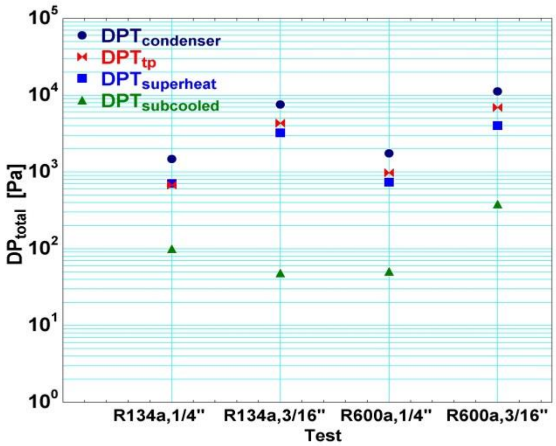

Figure 9. The total pressure drop for all zones.

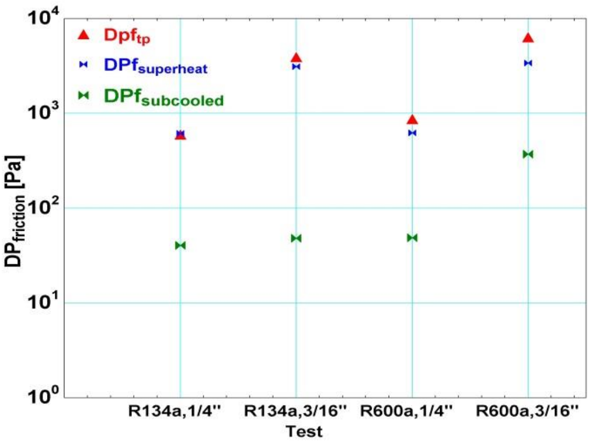

Figure 10. The friction pressure drop for all zones.

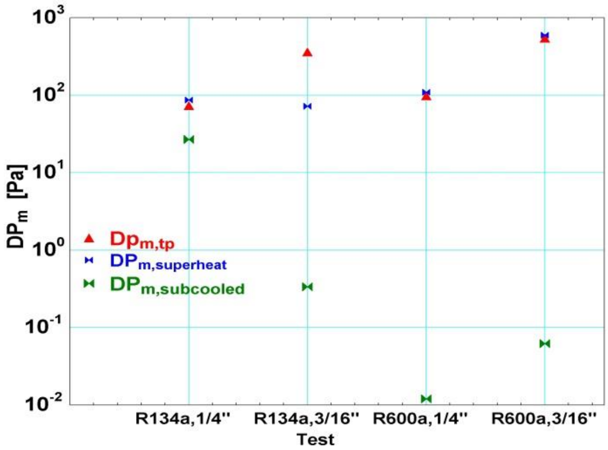

Figure 11. The momentum pressure drop for all zones.

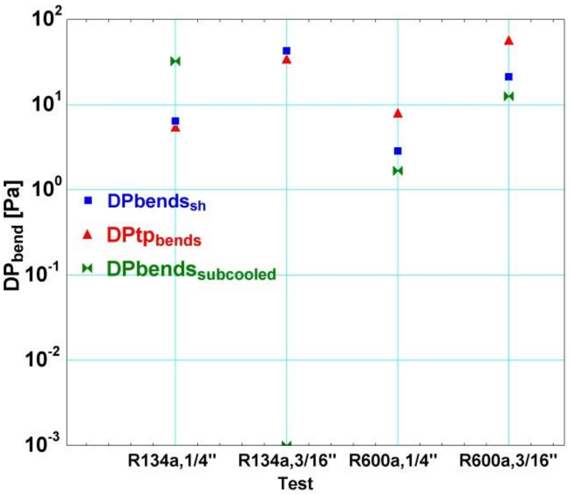

Figure 12. The bends pressure drop for all zones.

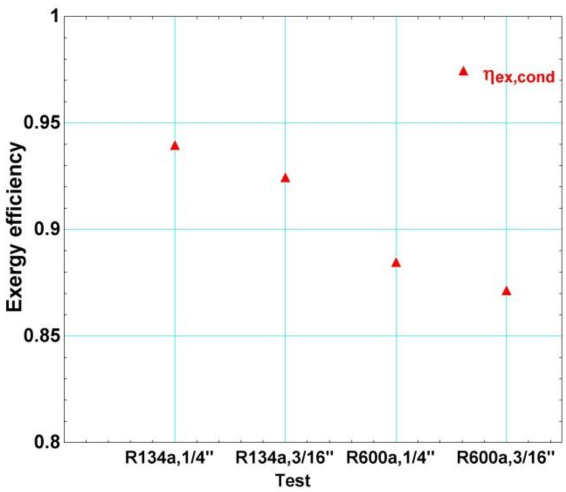

Figure 13. The exergy efficiency for the condenser.

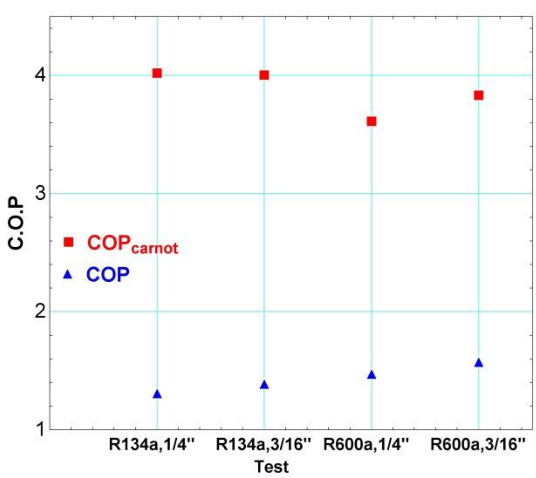

Figure 14. The C.O.P and C.O.P Carnot with tests.

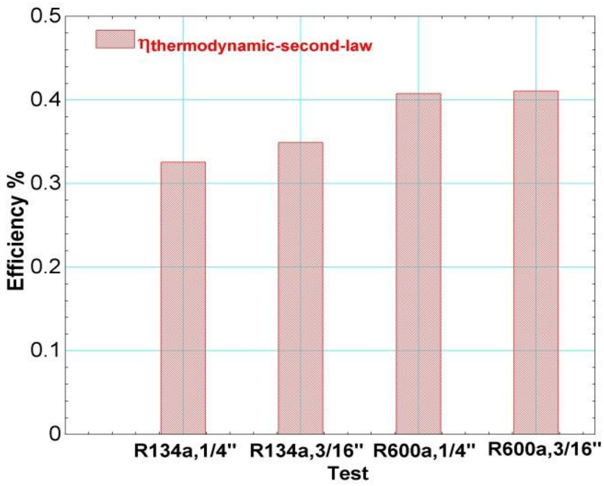

Figure 15. The second law thermodynamic efficiency.

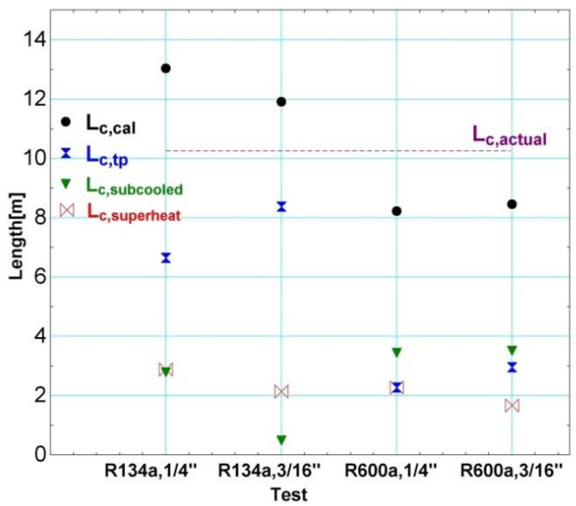

Figure 16. The length of condenser for all zones.

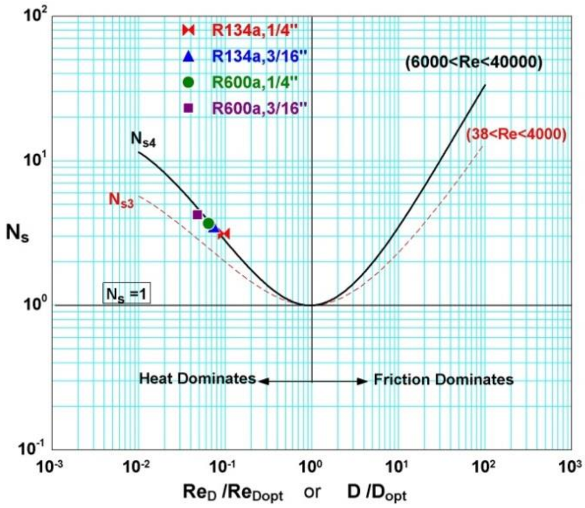

Figure 17. The optimum air flow of outer tube diameter condenser.

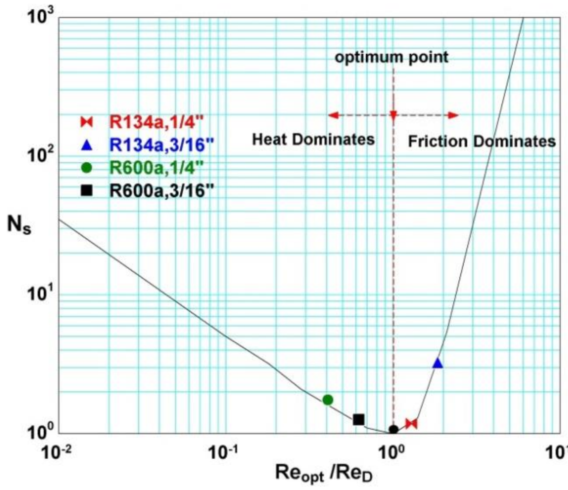

Figure 18. The optimum refrigerant flow of inner tube diameter condenser.

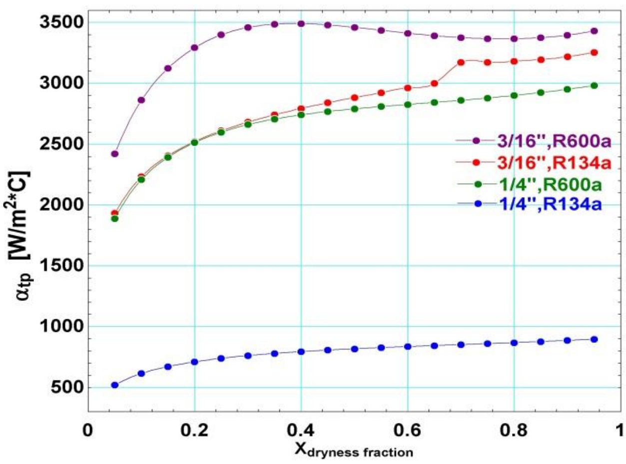

Figure 19. The relation between the heat transfer coefficient and dryness fraction

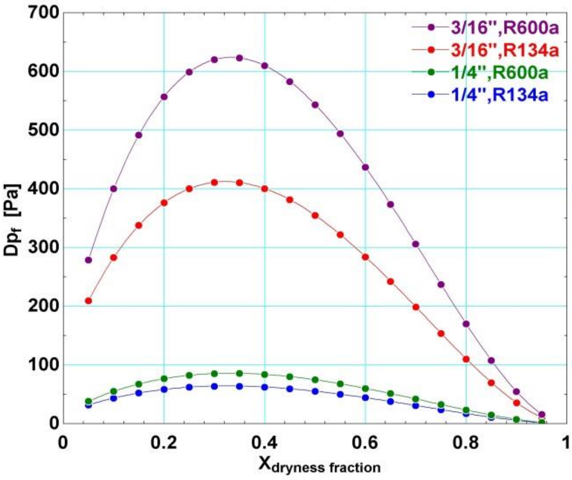

Figure 20. The relation between the friction pressure drop and dryness fraction.

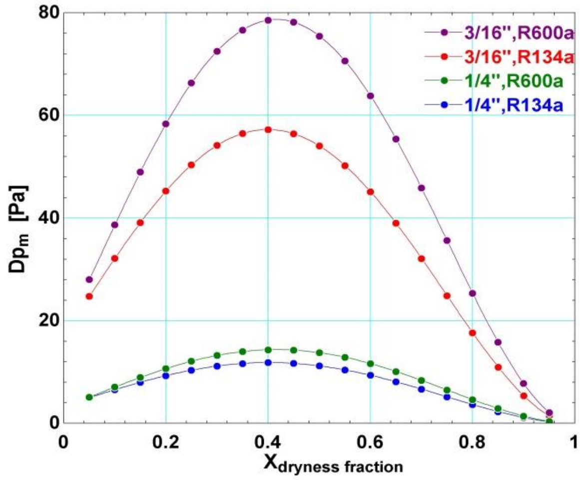

Figure 21. The relation between the momentum pressure drop and dryness fraction

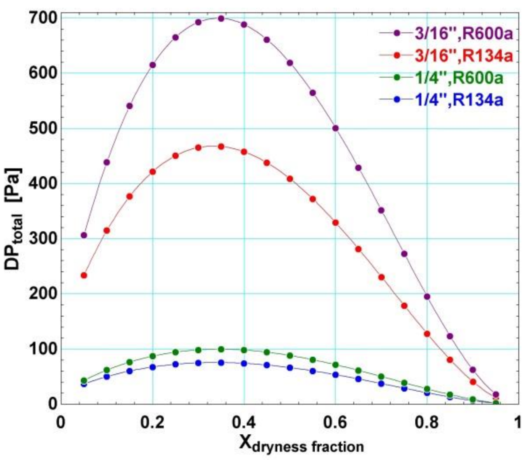

Figure 22. The relation between the total pressure drop and dryness fraction.

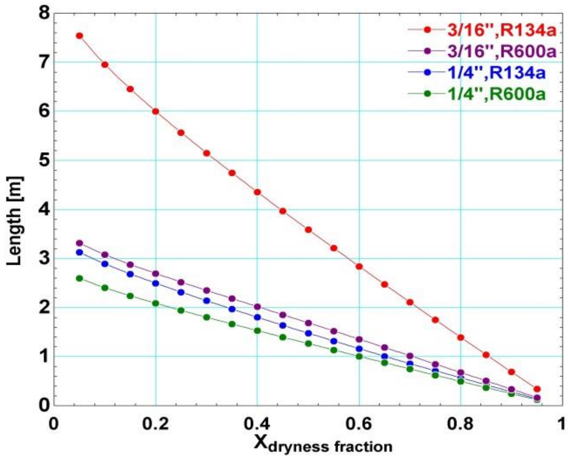

Figure 23. The relation between the Length of condenser and dryness fraction.

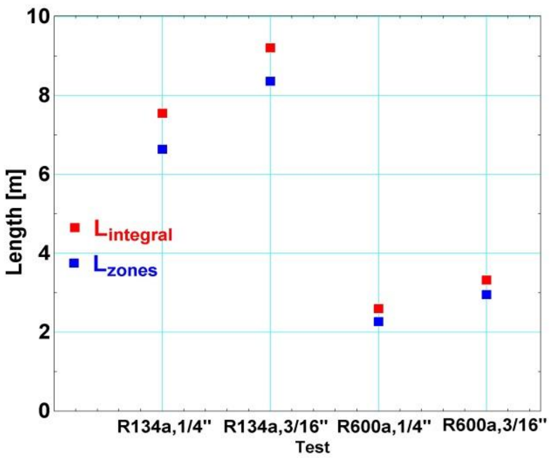

Figure 24. The comparison between the length calculated by zone method and the length calculated by integral method.

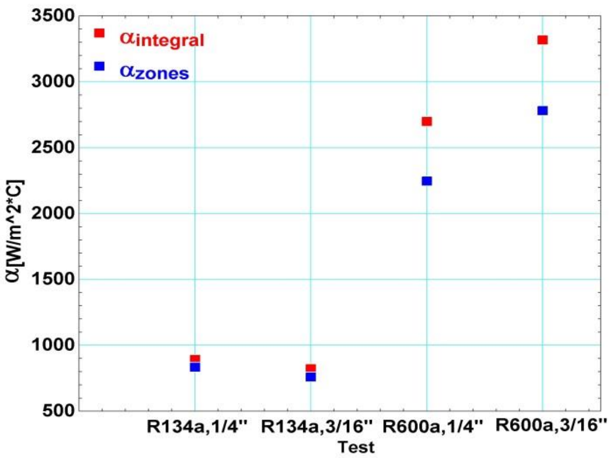

Figure 25. The comparison between the heat transfer coefficients calculated by zone method and integral method.

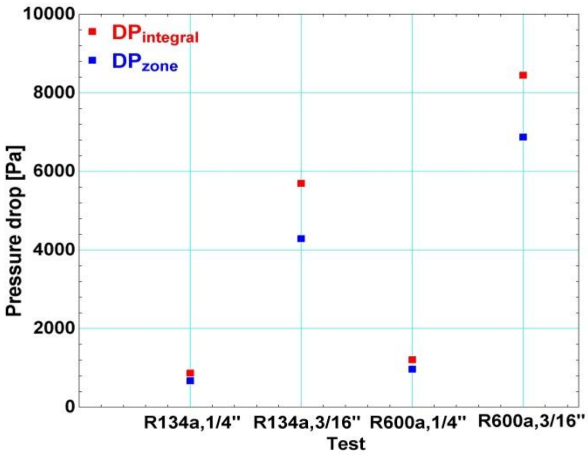

Figure 26. The comparison between the pressure drop calculated by zone method and the pressure drop calculated by integral method.

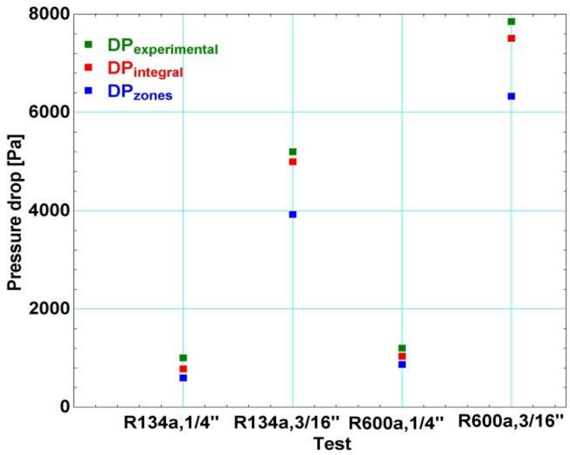

Figure 27. The comparison between the pressure drop from experimental work, integral method, and zone method.

6. CONCLUSIONS

The following concluding remarks are drawn from the tests:

1. The heat transfer coefficient calculated in the condenser for the test working with the refrigerant R-600a and tube diameter of condenser 4.76 mm is higher than the other tests.
2. The pressure drop of the condenser for the tests two (R-134a, 4.76 mm) and four (R-600a, 4.76 mm) is higher than the other tests.
3. The length of condenser required to remove the heat to the environment for tests working with fluid R-600a is smaller than the tests working with R-134a.
4. The optimum inner diameter of the condenser for the system working with R-134a is 6.35 mm, and the optimum inner diameter of the condenser for the system working with R-600a is 4.76 mm.
5. The optimum outer diameter of the condenser for all tests is the large exterior area.
6. The zone method was found slightly deviated from the integral method which approved that the current model for the zone method had a good agreement with integral method; that means the zone method is easy and reliable.
7. The integral method is more accurate than the zone method by 14%.

REFERENCES:

- A. S. H. R. A. E Fundamental, 1997, ASHRAE Handbook. ASHRAE, Atlanta.
- A. S. H. R. A. E Fundamental, 2006, ASHRAE Handbook. Refrigerant Part, Ch, 48, PP.7, ASHRAE, Atlanta.
- Bansal, and Chin, 2003, Modelling and Optimization of Wire-and-Tube Condenser, International Journal of Refrigeration Vol. 26, PP. 601-613.
- Bruce., R.M., Donald., F.Y., 2002, Fundamentals of fluid mechanics. John Wiley & Sons, Inc.
- Bejan, A., 1996, Entropy generation minimization, CRC Press, New York.
- Bejan, A., 2006, Advanced Engineering Thermodynamics Third Edition Handbook Ch.11, Wiley, Technology & Engineering.
- Dagilis, V., and Hofmanas, I., 2012, Influence of Surrounding Space on Heat Transfer Effectiveness of Refrigerators Condenser, ISSN 1392 -1207. MECHANIKA. Volume 18(3)

PP. 323-329.

- Dobson, M.K., Chato, J.C., Wattelet, J.P., Gaibel, J.A., Ponchner, M., Kenney, P.J., Shimon, R.L., Villaneuva, T.C., Rhines, N.L., Sweeney, K.A., Allen, D.G., and Hershberger, T.T., 1994,Heat transfer and flow regimes during condensation in horizontal tube, University of Illinois, Mechanical & Industrial Eng. Dept., Airconditioning and refrigeration center, ACRC TR-57. May.
- Domanski, P., and Hermes C. J. L. (2008). An Improved Correlation for Two-Phase Pressure Drop of R-22 and R- 410A In 180 Return Bends. Applied Thermal Engineering, 28, pp. 793–800.
- Hajal, J. El, Thome, J. R., and Cavallini, A. 2003, Condensation in Horizontal Tubes, Part 1: Two-Phase Flow Pattern Map, Vol. 46, PP. 3349-3363.
- Heo, J. H., Chae, M. S., and Chung, B. J., 2012, Influences of Vertical and Horizontal Pitches on the Natural Convection of Two Staggered Cylinders, International Journal of Heat and Mass Transfer, Volume 57, PP. 1-8.
- Holman, J. P., 2010; Heat Transfer, Textbook, 758.
- Lee, H. S., and Son, C. H., 2010, Condensation Heat Transfer and Pressure Drop Characteristics of R-290, R-600a, R-134a and R-22 in Horizontal Tubes, Heat and Mass Transfer 46(5) PP. 571-584.
- Mahdi, L. A., 2018, Entropy Generation Minimization Theoretical Analysis for External Flow around Horizontal Cylinder at low Reynold Number, Engineering and Technology Journal, Vol. 36, Part A, No. 2, pp. 202-206.
- Melo, C., and Hermes, 2009, A Heat Transfer Correlation for Natural Draft Wire-and-Tube Condenser, International Journal of Refrigeration, Volume 32, PP. 546-555.
- Muller-Steinhagen, H., and Heck, K., 1986, a Simple Friction Pressure Drop Correlation for Two-Phase Flow in Pipes. Chemical Engineering Progress, Vol. 20, PP. 297-308.
- Ragazzi, F., and Pedersen, C. O., 1991, Modular-Based Computer Simulation of an Air Cooled Condenser, University of Illinois, Mechanical & Industrial Engineering Dept. (217), 333-3115.
- Tanda, G., and Tagliafico, L., 1997, Free Convection Heat Transfer from Wire-and-Tube Heat Exchangers, J. Heat Transfer Vol. 119(2), PP. 370-372.
- Traviss, D.P., 1972, Condensation in refrigeration condensers, Ph.D thesis, Massachusetts Institute of Technology.

NOMENCLATURE

Symbol	Definition	Unit
A	Area	m^2
B	Constant	
B_o	Parameter	
a,b	Kays & London power coefficient	
C	Thermal capacitance ($\dot{m}$*C_p)	kW/K
C*	Thermal capacitance ratio Cmin/Cmax	
C_p	Specific heat at constant pressure	kJ/kg.K
D	Diameter	m
ED	Exergy destruction	W
ex	Exergy	J/kg
Fr	Froude number	
f	Friction factor	
f_i	Interfacial roughness factor	
G	Total mass velocity of liquid and vapor	$kg/m^2.s$
g	Gravitational acceleration	m/s^2
h_L	Liquid height	m
h_Ld	Dimensionless liquid height	
hfg	Latent heat	J/kg
h_n	Enthalpy at state n (n=1,2,3 …)	kJ/kg
k	Thermal conductivity	W/m.℃
L	Length of tube	m
$\dot{m}$	Mass flow rate	kg/s
Nu	Nusselt number	---
NTU	Number of transfer unit	---
p	Pressure	kPa
P	Power	W

Pr	Prandtl number	---
p_i	Perimeter of liquid-vapor interface	m
p_{id}	Dimensionless perimeter of interface	m
p_L	Wetted perimeter	m
Q	Heat transfer rate	W
Ra	Rayleigh number	---
Re	Reynolds number	---
r	Radius	m
St	Stanton number	---
S	Entropy	kJ/kg.K
S_{gen}	Entropy generation rate	W/K
T	Temperature	℃
t_{fin}	Fin thickness	m
u	Mean velocity	m/s
UA	Overall heat transfer coefficient	W/K
W	Work	W
We	Weber Number	---
x	Quality or dryness fraction	---

GREEK CHARACTERS

Symbol	Definition	Unit
α	heat transfer coefficient	$W/m^2.$ ℃
α_{tp}	Two phase local heat transfer coefficient	W/m2. ℃
α_a	Air-side average convective heat transfer coefficient	$W/m^2.$ ℃
α_r	Refrigerant side average convective heat transfer coefficient	$W/m^2.$ ℃
β	Extend coefficient for air in natural convection	1/K
β_o	duty parameter number	---
ϵ	Emissivity	---
ε	void fraction	---
δ	Liquid film thickness	m
η	Efficiency	---
η_{fin}	Fin efficiency	---
η_s	Air-side surface efficiency	---
ρ	Density	kg/m3
σ	Surface tension	N/m
σ_B	Stefan-Boltzmann constant	---
θ	The upper angle of the tube not wetted by stratified liquid	rad
θ_{strat}	Stratified angle	rad
ζ	Exergy dissipation	---
ξ	Factor	---
Λ	Factor in Müller-Steinhagen and Heck correlation.	

SUBSCRIPTS

Symbol	Definition
a	Air
amb	Ambient
dis	Discharge
g	Gas
go	Gas only
H	Homogeneous
h	Hydraulic
i	In
l	Liquid state
Ld	Dimensionless liquid
Lo	Liquid only
max	Maximum
min	Minimum
mist	Mist flow
o	out
r	Refrigerant
s	Surface
sat	Saturation
sub	Sub-cool
sh	Super-heat
strat	Stratified flow
suc	Suction
tot	Total
tp	Two phase
t	Tube
Π	Second law of thermodynamics
v	Vapor